Numerical wall-shape optimization for laminar flow in corrugated pipes

EINDHOVEN UNIVERSITY OF TECHNOLOGY
Department of Mathematics and Computer Science

CASA-Report 11-17
February 2011

Numerical wall-shape optimization for laminar flow in corrugated pipes

by

P.I. Rosen Esquivel, J.H.M. ten Thije Boonkkamp,
J.A.M. Dam, R.M.M. Mattheij

Centre for Analysis, Scientific computing and Applications
Department of Mathematics and Computer Science
Eindhoven University of Technology
P.O. Box 513
5600 MB Eindhoven, The Netherlands
ISSN: 0926-4507

Proceedings of ASME-JSME-KSME Joint Fluids Engineering Conference 2011
AJK2011-FED
July 24-29, 2011, Hamamatsu, Shizuoka, JAPAN

AJK2011-03044

NUMERICAL WALL-SHAPE OPTIMIZATION FOR LAMINAR FLOW IN CORRUGATED PIPES

Patricio I. Rosen Esquivel*
CASA†
Dept. of Math. and Comp. Science
Eindhoven University of Technology
Eindhoven, The Netherlands
Email: p.i.rosenesquivel@tue.nl

Jan H.M. ten Thije Boonkkamp
CASA
Dept. of Math. and Comp. Science
Eindhoven University of Technology
Eindhoven, The Netherlands
Email: tenthije@win.tue.nl

Jacques A.M. Dam
Imtech SMS
The Hague, The Netherlands
Email: jacques.dam@imtech.nl

Robert M.M. Mattheij
CASA
Dept. of Math. and Comp. Science
Eindhoven University of Technology
Eindhoven, The Netherlands
Email: r.m.m.mattheij@tue.nl

ABSTRACT

In this paper we address the problem of wall-shape optimization for axially symmetric corrugated pipes. The main objective is, to increase the flow rate in a periodic section of a pipe, by modifying the wall-shape from the traditional cylindrical shape. We tackle this problem by numerically solving the Navier-Stokes equations for the periodic section of the pipe. The numerical model is validated by comparing our numerical results with available experimental data on the pressure drop and friction factor.

The wall-shape optimization problem is tackled by considering a family of periodic pipes, in which the wall-shape is characterized by the amplitude, and the ratio between the lengths of expansion and contraction of the periodic section. We first study the effects of varying these parameters and then we show that for small Reynolds numbers the optimal shape turns out to be symmetric, while for large Reynolds numbers, a configuration with a large expansion region, followed by a short contraction region, performs better. The dependency of the optimal ratio on the pressure gradient is studied, and at the same time, we quantify the improvement in terms of flow rate (reduction in friction). Depending on the kind of geometry and the applied pressure gradient, the flow rate can be increased by 8%*, for a geometry with small period. In the case of a geometry with large period, the flow rate increases by* 35%*, for large Reynolds number, and even* 120% *for small Reynolds numbers.*

1 INTRODUCTION

The effect of wall shape on the friction factor of forced flow through pipes and hoses is of interest in many applications such as in the LNG industry [1]. The study of flow in non-straight pipes dates back to Nikuradse's experiments [2], whose results obtained from artificially roughened pipes, were later arranged in the more well-known form of the Moody Diagram [3], where for laminar flow, the friction factor is usually shown as independent of the roughness. Despite this, several numerical and experimental studies have shown that the contribution of wall shape is not

*Address all correspondence to this author.
†Centre for Analysis, Scientific Computing and Applications.

trivial, even in the laminar case. This happens specially when dealing with a wall-shape, rather than just with some random roughness [4–6].

In this paper, we study the effects of wall-shape on the flow, and consider the possibility of finding a wall-shape that maximizes the flow rate for a given pressure gradient. We do this by first presenting the governing equations, the geometry under consideration, at this point we distinguish between two study cases, the *cavity* configuration, and the *slowly varying* configuration. Second we recall the problem of flow in a straight pipe, and show a formalism for handling pipes with varying cross section. After this, we start the discussion on the implementation of the numerical model, and present a comparison with experimental data, for validating our model.

Based on the experiment for validation, we start the discussion on the effects for each of the geometrical parameters, and we also discuss the influence of the Reynolds number. We present the results for the *cavity* configuration, and for the *slowly varying* geometry. The role of each of the parameters in each case is discussed in detail. In both cases it turns out possible to increase the flow rate, and the situation looks specially promising for the *slowly varying* geometry, where and improvement of up to 120% was observed. When dealing with large pressure gradients, an asymmetric wall-shape can perform better than the symmetric counterpart. We study the dependency of the optimal ratio of expansion and contraction, on the pressure gradient. Finally we summarize the results in the conclusions section.

2 GOVERNING EQUATIONS AND GEOMETRY

We consider the Navier-Stokes equations for steady, incompressible, axially symmetric, laminar flow in cylindrical coordinates

$$UU_X + VU_R = \nu\left(U_{XX} + U_{RR} + \frac{1}{R}U_R\right) - \frac{1}{\rho}P_X, \tag{1a}$$

$$UV_X + VV_R = \nu\left(V_{XX} + V_{RR} + \frac{1}{R}V_R - \frac{1}{R^2}V\right) - \frac{1}{\rho}P_R, \tag{1b}$$

$$U_X + V_R + \frac{1}{R}V = 0, \tag{1c}$$

where the corresponding variables are the axial coordinate X, the radial coordinate R, the axial velocity U, the radial velocity V, and the pressure P. The constants ν and ρ represents the kinematic viscosity and the density of the fluid, respectively. The angular component does not play a role due to the assumption of axially symmetric flow.

In Figure 1, we see an example of a corrugated pipe. This particular variant corresponds to a typical design of LNG transfer pipes. This particular geometry is not axially symmetric,

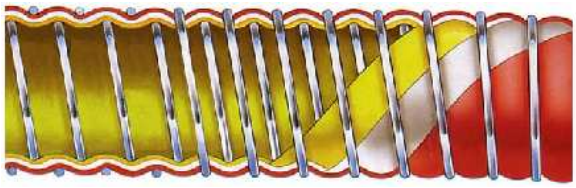

FIGURE 1. Typical construction design for flexible corrugated pipes. Image taken from [8, pp. 6].

but there are also other kind of constructions in which the final product is axially symmetric indeed [7]. In any case, the axially symmetric version constitutes an approximation for geometries like this one. Under the assumption of axial symmetry, the location of the wall of the pipe can be described in terms of the cylindrical basis vectors $\mathbf{e}_R$, $\mathbf{e}_\Theta$, $\mathbf{e}_X$, via the parametrization $\mathbf{X}(\Theta, X) = \tilde{R}(X)\mathbf{e}_R + X\mathbf{e}_X$, with parameters $0 \leq \Theta < 2\pi$, $0 \leq X \leq L$. As boundary conditions we consider no-slip at the wall of the pipe, i.e.,

$$U(X, \tilde{R}(X)) = V(X, \tilde{R}(X)) = 0, \quad 0 \leq X \leq L, \tag{2a}$$

(2b)

We also require boundary conditions at the inlet and outlet of the periodic section. But we will discuss these in the next section.

2.1 The Darcy Friction Factor

A quantity of interest in the analysis of pipe flow is the so-called pressure drop. In the particular case of flow in a straight pipe, the pressure drop is directly related to the mean flow rate, and it determines the power requirements of the device to maintain the flow. In practice, it is convenient to express the pressure loss as follows [9]

$$\Delta P = f\frac{L}{D}\frac{\rho\bar{U}_0^2}{2}, \tag{3}$$

where, $\Delta P = P_{\text{in}} - P_{\text{out}}$ is the pressure drop over a segment of length L, f is the Darcy friction factor, D is the diameter of the pipe, ρ is the density and $\bar{U}_0$ is the average of the velocity over the cross section. In the case of laminar flow, i.e., for Poiseuille flow, the friction factor takes the form

$$f_{\text{sp}} = \frac{64}{\text{Re}}, \tag{4}$$

where Re is the Reynolds number, defined as

$$\text{Re} := \frac{\bar{U}_0 D}{\nu}. \tag{5}$$

The flow rate in a straight pipe Q_{sp}, can then be expressed as

$$Q_{\text{sp}} = \frac{\Delta P \pi D^4}{128 \mu L} = \frac{\pi}{8\mu} \beta R^4, \tag{6}$$

where μ is the viscosity, $\nu = \mu/\rho$ the kinematic viscosity, R the radius of the pipe, and $\beta = \Delta P/L$ the mean pressure gradient. The previous holds for the special case of fully developed flow in straight pipes; we have added the subindex sp in (6) and (4), to indicate this. These values will be used later as reference for comparing the flow rates obtained in corrugated pipes.

When we deal with pipes with non-constant radius, but periodic, it is still possible to link the pressure drop to the losses of mechanical energy in the flow [10]. This can be done, by considering the changes in the flow along a periodic section of the pipe. Of course, since the radius of the pipe is not constant, we need to choose a characteristic radius and average velocity. In this paper we select the respective values at the inlet of the pipe, i.e., $D = 2\tilde{R}(0)$ and,

$$\bar{U_0} = \frac{1}{\pi \tilde{R}^2(0)} \int_{\Gamma_{\text{in}}} U \, \text{dS} = \frac{Q}{\pi \tilde{R}^2(0)}, \tag{7}$$

where Q is the flow rate over a cross section. Notice that due to incompressibility, the value of Q is the same at any cross section. The expression in (3) can then be used as a lumped model for describing the flow in any periodic pipe, where now ΔP represents the pressure drop over one period, and L the period of the pipe.

It is also important to mention, that when the flow is not fully developed, or when the pipe is not periodic, the total losses of mechanical energy cannot be related to the pressure drop. In this case, Herwig et.al [10,11], proposed an alternative approach, which allows to obtain the friction factor (or more generally the head loss coefficient) of any kind of hydraulic component. Their approach is based on computing the local dissipation rate over the whole domain. Then, in a postprocessing step, the dissipation rate is integrated over the domain, in order to obtain the total energy dissipated by the flow. In the particular case of fully developed flow in periodic pipes, both approaches coincide, and therefore we will consider the approach based on the pressure drop presented above.

2.2 Wall-shape of a Pipe Section

The main goal of this paper is to characterize the effects of wall-shape on the flow and to study the possibility of designing a wall-shape that maximizes the flow rate for a given pressure gradient. In order to explore the effects of wall shape, we will consider a piecewise sinusoidal pipe depicted as in Figure 2 [12]. The shape consists of two sinusoidal shapes with amplitude a, and with periods $2E$ and $2C$ in the expansion and contraction regions, respectively. These sections are matched at $X = E$, in such a way that both $\tilde{R}$ and $\tilde{R}'$ are continuous everywhere. The geometry considered here, has already been scaled, having the minimum radius of the pipe $\tilde{R}(0) = 1$. The resulting period of the pipe L, results from adding the length of the expansion region E, with the length of the contraction region C.

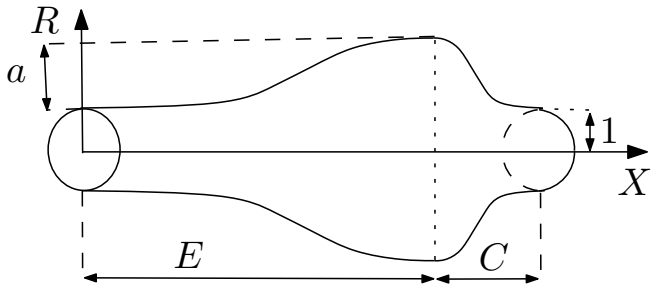

FIGURE 2. Periodic section of a pipe with center line along the X-axis, a represents the amplitude of the pipe, E the length of the expansion region, C the length of contraction region. The period L of the pipe, satisfies $L = E + C$.

To classify the geometry, we will use the amplitude of the pipe a, the period of the pipe L, and the quotient L_e of the length of the expansion region over the length of the period, which is defined as

$$L_e := \frac{E}{L}. \tag{8}$$

These coefficients completely define the geometry, and also allow us to distinguish between two essentially different, geometric configurations. The categories we will refer to, are the *Cavity* configuration, i.e., $L \ll 1$, and the *Slowly Varying* configuration, which appears when $L \gg 1$. As we will show later, these two configurations exhibit substantial differences in the flow behavior. For example, in the slowly varying case, the parameter L_e plays a more important role on the final flow rate, than in the cavity case. This classification, basically allows us to identify the cases, in which wall shape optimization can deliver a significant increase on the flow rate.

3 Numerical Methodology

In the particular case of fully developed flow, it is possible to reduce the computation domain of a corrugated pipe to just one period. This can be explained using the following argument. Since the geometry under consideration is periodic, it is plausible to assume that all velocity components are periodic as well. On the other hand, although the pressure is certainly not periodic, we

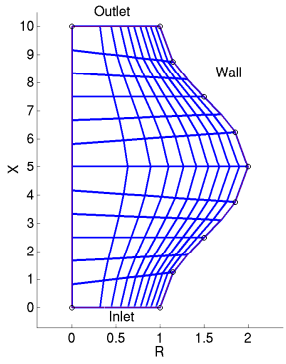

FIGURE 3. Mapped mesh for a sinusoidal pipe with 12 elements in the axial direction X, and 10 elements in the radial direction

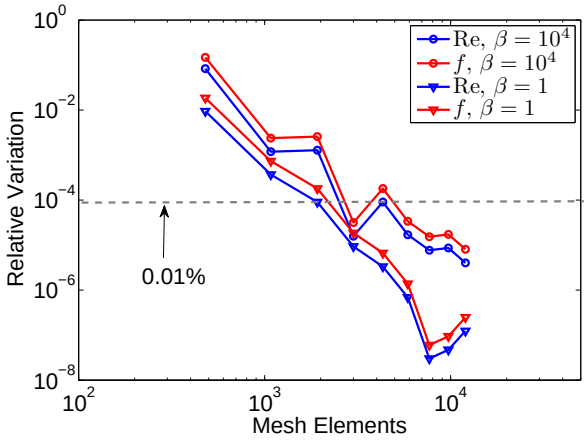

FIGURE 4. Relative changes in the computed Reynolds number Re and friction factor f, for two different pressure gradients $\beta = 10^4, 1$.

can still decompose the pressure as follows

$$P(X,R) = \tilde{P}(X,R) + \beta X, \tag{9}$$

where $\tilde{P}(X,R)$ represents the fluctuations due to the presence of the corrugation, and β is the mean pressure gradient.

This transformation has been frequently used in the literature [13–16], and the main advantage of this reformulation is that the new function $\tilde{P}$ is also periodic, thus allowing to reduce the computational domain to just one period. Notice that we solve for the pressure fluctuation $\tilde{P}$, instead of for the original pressure P, nonetheless, this is valid because the Navier-Stokes equations only involve the gradient of the pressure, and not the pressure itself.

The implementation works in the following way. First, we prescribe a pressure gradient β, i.e., a total pressure drop of $\Delta P = \beta L$ in one periodic section of the pipe. Second, we include the mean pressure gradient β as a force term in the Navier-Stokes equations, with variables U, V and $\tilde{P}$, and solve these equations numerically. Finally we compute the average velocity $\bar{U}_0$ and the flow rate Q, by integrating the axial velocity component U over the inlet of the pipe, which allows us to compute the resulting Reynolds number Re, and friction factor f, according to

$$\mathrm{Re} = \bar{U}_0 D/\nu = \frac{2Q}{\pi \nu R}, \quad f = \beta \frac{2D}{\rho \bar{U}_0^2}. \tag{10}$$

The Navier-Stokes equations are solved with a mixed finite element model, with Lagrange P_2, P_1 elements, i.e., the velocity is approximated with quadratic elements, and the pressure with linear elements. The order of approximation of the pressure is chosen to be one order less than for the velocity, in order to avoid an overdetermined system of discrete equations [17]. The model used for these simulations, was implemented with the code Comsol Multiphysics [18].

The mesh used for discretizing the geometries studied in this paper, is a mapped-mesh of quadrilateral elements, see Figure 3. The distribution of the elements in the axial direction is uniform, while in the radial direction, the density of the elements increases quadratically when approaching the wall. The mesh is designed to be finer close to the wall, in order to be able capture the strong gradients of the velocity field near the protrusion. The mesh was chosen to be coarser close to the center line, in order to reduce the calculation time.

It is also important to mention, that by using a mapped mesh, is is possible to obtain grid independent solutions at much smaller computational costs than with other alternatives, such as the boundary layer type mesh, which consists of an mesh of quadrilateral elements close to the boundary, and a uniform triangular mesh in the core region. This is particularly the case, for the geometry in the *cavity* category. This happens, because in order to accurately solve for the vortex (or vortices) that form inside the protrusion, the boundary layer mesh needs to be refined many times.

In order to obtain grid independent solutions, the calculations were performed for different mapped meshes, until a new refinement provided no significant changes in the solution nor in the variables of interest, namely Re, Q, and f. In Figure 4 we can observe the absolute value of the relative variations of the computed Reynolds number Re, and friction factor f, versus the total number of elements in the mesh. Notice that due to (10) an accurate value for Re implies an accurate value for Q, and therefore we do not need to check for its accuracy. For the construction of this plot, the initial number of elements in the axial and in the radial directions were 12 and 10, respectively, and subsequently, the number of elements in each direction was increased linearly

until a further increase produced a change of less than 0.01% for the Reynolds number Re, and the friction factor f. For the case of a pressure gradient $\beta = 1$(triangle markers), a variation of less than 0.01% in the Reynolds number Re is attained at a mesh with 48 elements in the axial direction and 40 elements in the radial direction, delivering a converged value of Re ≈ 0.6807. On the other hand, the friction factor f requires a mesh with 60×50 elements to present a variation of less than 0.01%, and converges to the value $f = 34.5304$. The number of elements increases with the mean pressure gradient β, and in order to obtain convergence for the case $\beta = 10^4$, we need a mesh with 84×70 elements. Of course, depending on the complexity of the geometry, the amount of elements required to achieve convergence increases. This is specially the case for the *cavity* configuration, but still a grid independent result is attained at much less cost than with a boundary layer mesh. In order to warrant grid independence for all geometries, we implemented a routine which recursively refines the mapped mesh, until the relative change in the computed friction factor was less than 0.01%. Once this condition is met, the Reynolds number (and consequently the flow rate), automatically satisfy the same condition, as it can be observed in Figure 4.

The discretized nonlinear system of equations is solved using Newton iteration, in combination with a zeroth order continuation for the mean pressure gradient β. This means that the solution computed at a given pressure gradient, is used as initial guess for the Newton iteration, at the next (higher) pressure gradient [17].

4 RESULTS AND DISCUSSION

Since it is always instructive to compare results with experimental data, in Figure 5 we show a plot of experimental data (blue dots) obtained by Deiber et al. [19, p. 642], and the corresponding values obtained with the numerical model described above (red triangles). The figure shows the friction factor versus the Reynolds number, for a symmetric sinusoidal pipe, which in terms of our parameters (see Figure 2), correspond to $a = 0.8571$, $L = 8.9714$ and $L_e = 0.5$. The additional straight line in the plot, was added in order to show that, starting from a certain value for Re, the friction factor deviates from a straight line. This is in agreement with the conclusions of other authors [19, 20].

The numerical model is able to accurately predict the friction factor up till Re ≈ 750.8, where a change towards turbulence can be observed from the experimental data. This point has been signaled with a "T" in Figure 5. For Re beyond this value, the steady state numerical model can not be expected to correctly describe the friction factor.

In order to have a better picture of the effects of the Reynolds number on the flow, in Figure 6 we present plots of the fluctuation of the pressure $\tilde{P}$, and the streamlines for this geometry, at different values of Re. The center line is located at $R = 0$, the

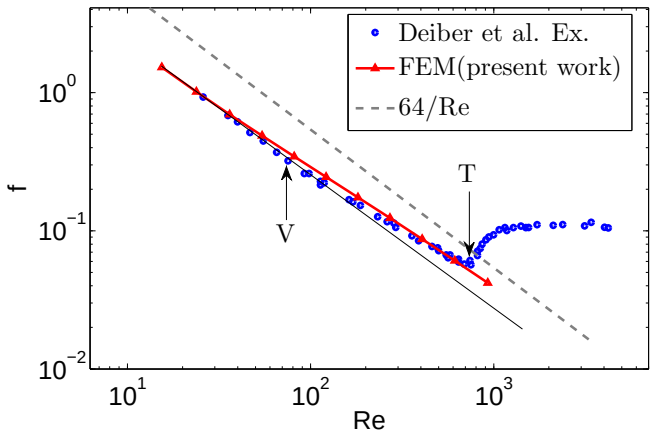

FIGURE 5. Experimental results (blue dots) for the friction factor by Deiber et al. [19, p. 642], and values obtained with FEM simulations (red line), as function of the Reynolds number, for a sinusoidal pipe with parameters $a = 0.8571$, $L = 8.9714$, and $L_e = 0.5$. All the values were converted from the variables used in Deiber et al. [19], to the ones used in this paper.

wall of the pipe appears on the right side of the picture, and the flow direction is upwards. For Re $= 36.15$ (Figure 6(a)), we can observe how the streamlines simply follow the wall of the pipe, and the pressure is almost constant along the cross sections. In Figure 6(b), at Re $= 81.33$, we can see pointed by an arrow, the onset of a vortex in the protrusion of the pipe, which is also signaled in Figure 5 with "V". This vortex increases size with Re, and in Figure 6(c), we can observe how the vortex almost fills the whole protrusion of the pipe, and how the pressure starts to be non-constant over cross sections, for instance at the cross section $X/\tilde{R}(0) = 7$. Although the experimental results at Re $= 927.7$ already exhibit a transition towards turbulence, it is still instructive to have a look at the results from the steady state numerical model. In Figure 6(d), we can observe how in this situation, the vortex completely fills the protrusion, and how it is squeezed by the core flow. As a result, the center of the vortex migrates further in the flow direction (see arrow), giving rise to a stagnation point. This can be observed from the variations of the pressure over cross sections.

From the discussion above, we see that the presence of a corrugated wall, can have a big influence on the flow pattern and on the friction factor as well. In fact, when compared to the friction factor of a straight pipe with radius 1 (dashed line in Figure 5), the friction factor of this wavy pipe, is about 50%, and 30% smaller, at Re ≈ 81.33, and Re $= 612.7$, respectively. Therefore, we would like to know in which cases is it possible to obtain such a reduction in the friction factor, and to know how this translates in terms of the flow rate Q. In case it is possible, we would like to find the set of optimal parameters a, L, and L_e,

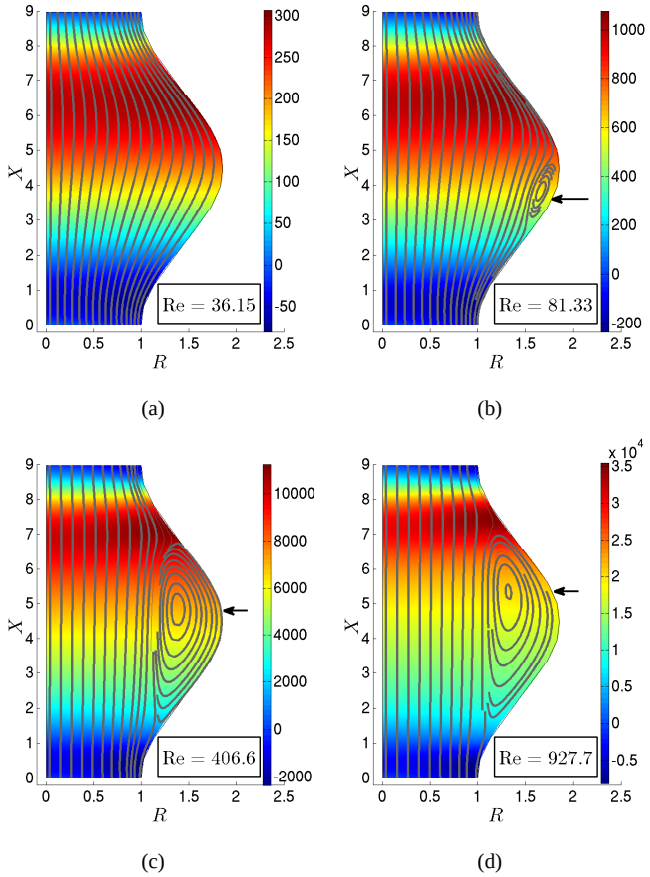

FIGURE 6. Pressure fluctuations $\tilde{P}$, and streamlines for a sinusoidal pipe with radius at inlet $\tilde{R}(0) = 1$, amplitude $a = 0.8571$, period $L = 8.9714$, $L_e = 0.5$ and various Reynolds numbers.

that maximizes the flow rate Q, for a given pressure gradient β.

4.1 The Cavity Configuration

Now we will analyze the effects of the parameters a and L_e, in the case of the cavity type configuration, i.e., $L \ll 1$. In our particular case, we consider a geometry which after scaling, corresponds to a sinusoidal pipe with parameters $L = 0.2666$, and $L_e = 0.5$. The wall shape of this pipe has an amplitude of $a = 0.1053$, but instead of only considering this fixed value, we will vary this parameter in order to characterize the effects.

In Figure 7, we present a plot of the flow rate Q, versus the mean pressure gradient β, for different values of a. All flow rates have been scaled by the reference flow rate Q_{sp}, which corresponds to the flow rate in a straight pipe with radius 1, see (6). From this figure, we can observe that for $a = L/5$, the flow rate is about 5.5% larger that in the reference straight pipe. This increment in the flow rate continues for increasing values of a, but the extra increment is every time smaller. For instance, when we

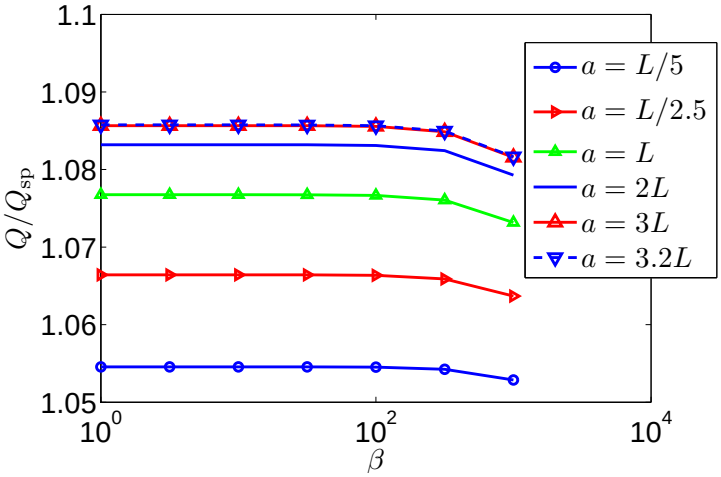

FIGURE 7. Flow rate Q as function of the applied pressure gradient β, for sinusoidal pipes with $L = 0.26$, $L_e = 0.5$, and several values of a. All values have been scaled with the reference flow rate Q_{sp} of a straight pipe with radius 1, see (6).

set $a = L$, the increment in flow rate is about 7.8%, whereas as if we set $a = 2L$ then the total increment in flow rate is about 8.3%, i.e., after increasing the amplitude twice, the extra increment we obtain is only 0.5%.

This numerical evidence, leads us to conclude that the flow rate always increases with the amplitude, and that the increase is every time smaller. Of course this statement is based on the assumption that the flow remains laminar. This condition is very important, because we can not expect this statement to hold for any arbitrary large Reynolds number. In case the flow exceeds the so-called critical Reynolds number, the flow is expected to become turbulent, and this implies an increase in friction and a reduction in flow rate as well. In fact, there is strong evidence that increasing the amplitude a, might cause a reduction of the value of the critical Reynolds number [21]. We can get some idea of why this might occur by looking at the changes in the flow pattern for different values of a. In Figure 8, we can observe the streamlines for a pipe with period $L = 0.26$, and different amplitudes. From this picture we can see how for the same Reynolds number ($\text{Re} \in [0.84, 0.85]$), the complexity of the flow increases with increasing a. For instance, when $a = L/2$ (Figure 8(a), we can observe a small vortex, when we increase the amplitude to $a = L$ (Figure 8(b)), and $a = 1.8L$ (Figure 8(e)), we can observe two and three vortices respectively.

Another interesting observation is that when a increases, the Reynolds number at which a vortex appears decreases. For example, at $a = L/5$ and $\text{Re} = 0.84$, the flow exhibits no vortex, whereas for $a = L/2$ and the same Reynolds number, in Figure 8(a) we can observe a small vortex. This vortex increases in size with Re, as we can observe in Figure 8(b). For the cases

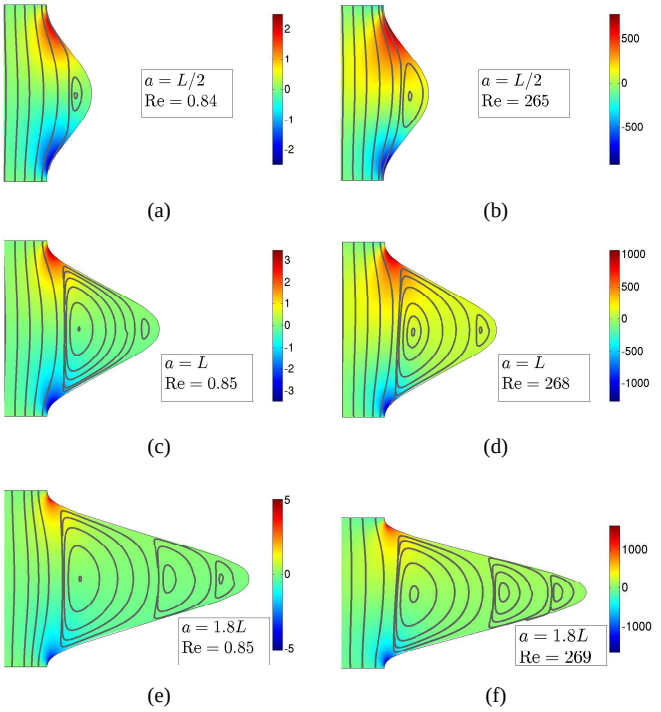

FIGURE 8. Pressure fluctuations $\tilde{P}$, and streamlines for a sinusoidal pipe with radius at inlet $\tilde{R}(0) = 1$, amplitude period $L = 0.26$, $L_e = 0.5$ and various amplitudes a. All pictures are in the same scale, and in order to display the vortices clearly, the left limits of all pictures start from $R = 0.9$. The flow direction is upwards.

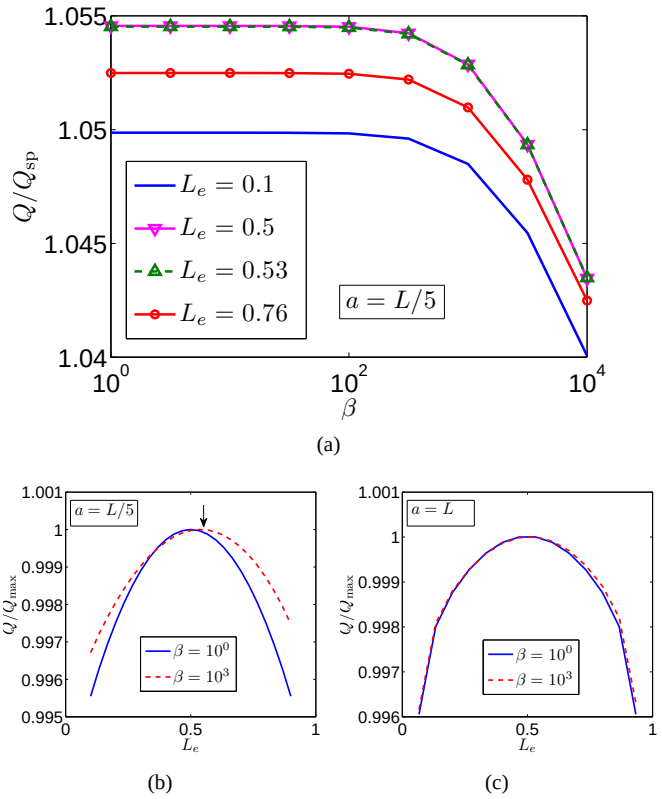

FIGURE 9. Figure 9(a) shows the flow rates, scaled with Q_{sp}, versus the pressure gradient β for different values of L_e. Figures 9(b),9(c), show the flow rates Q, as function of L_e.Here the flow rates were scaled with the maximum flow rate Q_{max} for each value of β. The parameter L in both figures is $L = 0.26$.

$a = L, 1.8L$, even when Re ≈ 0.85 the vortices completely fill the protrusion of the pipe. In these cases, the effect of increasing Re is that the vortex in "contact" with the core is squeezed, and as a consequence it looses symmetry. A similar effect can been observed for the pressure field, which is antisymmetric with respect to $X = L/2$, at Re $= 0.85$ and it looses this property for higher Reynolds numbers Re $= 265, 268$ in Figures 8(b), 8(d).

Now we study the influence of the parameter L_e. In Figure 9(a) we have plotted the flow rate, scaled by Q_{sp}, for a fixed amplitude $a = L/5$ and various values for L_e.As we can see, L_e does not play a very important role in this configuration, and changing L_e from the value 0.5 to another value, appears to be detrimental. For instance, setting $L_e = 0.1$, reduces our original increase in flow rate from 5.5%, to 5%, and a similar effect can be observed when we set $L_e = 0.76$. But this is not always true, in fact, for $\beta = 10^3$, setting $L_e = 0.53$ delivers a small improvement. In order to see this clearly, for each value of β, we have normalized the flow rates by the maximum flow rate, and we have plotted this normalized flow rate versus the parameter L_e, for different values of β in Figure 9(b). For $\beta = 1$, the flow rate is symmetric with respect to $L_e = 0.5$, and at this point the maximum flow rate is attained. When $\beta = 10^3$, the flow rate shows an asymmetric shape, and the optimal value shifts to $L_e = 0.53$, which is indicated by an arrow. Unfortunately, as we can see from Figure 9(a), the additional increment in flow rate is very small.

The situation becomes even more hopeless for larger values of a. In Figure 9(c), we can see the normalized flow rates for $a = L$. From this picture, we can clearly see that even for $\beta = 10^3$, the curve for the flow rate remains symmetric and the optimum is attained at $L_e = 0.5$. For the cavity configuration, the parameter L_e, can only give some improvement when a is small, but this improvement is so small, that in practice it is simply better to set $L_e = 0.5$. In the next section, we will see that the situation is different for the slowly varying configuration.

4.2 The Slowly Varying Configuration

Now we study the effects of the parameters a, and L_e for the slowly varying configuration. To this extend, we consider a family of sinusoidal pipes with parameter $L = 5$. As in the case of the cavity configuration, we study first the effect of varying the am-

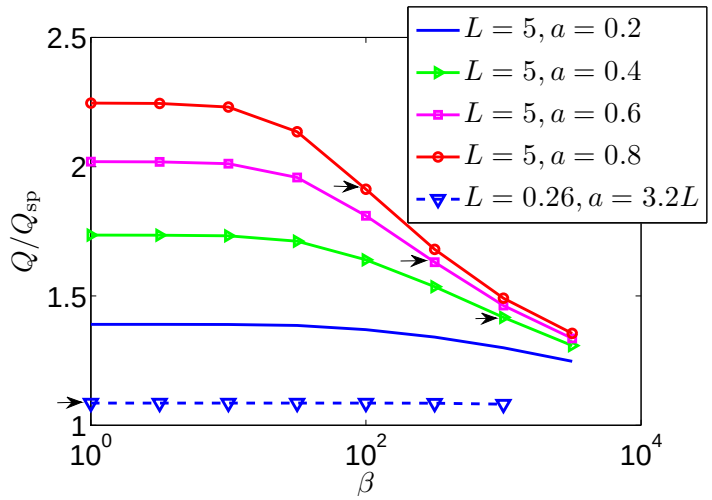

FIGURE 10. Flow rate Q as function of the applied pressure gradient β, for sinusoidal pipes with $L = 5$, $L_e = 0.5$, and several values of a. All values have been scaled with the reference flow rate Q_{sp} of a straight pipe with radius 1, see (6). For comparison, the configuration with largest flow rate from Figure 7 (blue triangles) has been added.

plitude a. In Figure 10, we can observe the obtained flow rate Q, scaled by Q_{sp}, versus the pressure gradient β, for different values of a. For comparison, we have added the curve with highest flow rate from the cavity configuration, i.e., the plot corresponding to the parameters $L = 0.26$, and $a = 3.2L = 0.83$ from Figure7. From this figure, we immediately realize that a has much more influence than in the case of the cavity configuration.

The increment in flow rate for the cavity geometry with parameters $L = 0.26$, and $a = 0.83$, delivers an increment of 8.6%, relative to a straight pipe. This increment is not very substantial when compared to the results obtained with the slowly varying geometries. For instance, when $L = 5$, and $a = 0.2$, the increment in flow rate is about 39%, for small values of β, and about 24% for the largest value of this parameter, namely $\beta = 10^{3.1}$ (Re = 985). Even though the amplitude in this slowly varying configuration is about one quarter of the amplitude in the cavity configuration, the increment in flow rate is between 2 and 5 times higher. This effect becomes much more prominent for larger values of a, going from a 73% increment for $a = 0.4$, to a 120% improvement for $a = 0.8$, for small pressure gradients. For the largest applied pressure gradient of $\beta = 10^{3.5}$, the increments in flow rate are 31%, 33%, and 35%, for the geometries with $a = 0.4$, $a = 0.6$, and $a = 0.8$, respectively.

If we concentrate only on the slowly varying geometries, again, as in the cavity configuration case, we can conclude that the flow rate always increases when the amplitude a increases. This increment show the same behavior, as in the cavity configuration case, and the extra increments are smaller each time. This effect becomes stronger for large values of β, as we can see

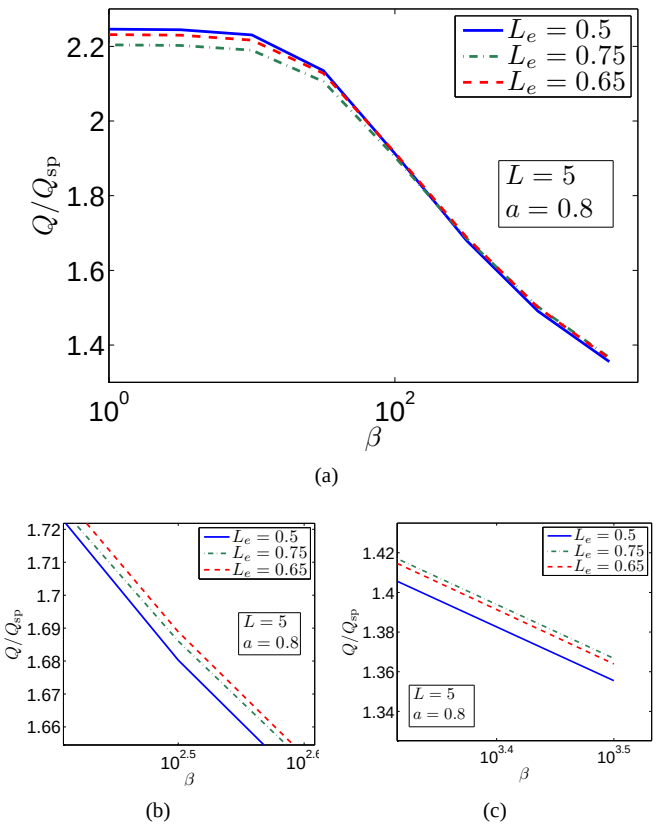

FIGURE 11. Figure 11(a) shows the flow rates, scaled with Q_{sp}, versus the pressure gradient β for different values of L_e. Figures 11(b), and 11(c), show the plot zoomed around $\beta = 10^{2.5}$, and $\beta = 10^{3.5}$ respectively. The parameter L was set to 5.

from Figure 10, this happens because as β becomes large, inertia effects become more important, and vortices are expected to appear. As reference, we have added small arrows in Figure 10, indicating the smallest value of β in which a vortex appears.

These simulations also suggest that the flow is more likely to remain laminar than in the cavity case. To see this, let us first recall that in the cavity case, for $a = L/2 = 0.13$, the Reynolds number at which a vortex appears is Re = 0.84 (see Figure 8). This value is much smaller, than the Re = 372 for the geometry with $L = 5$, and $a = 0.4$. This basically means that the assumption of laminar flow holds in a larger range of Re.

Now we turn our attention to study the influence of the parameter L_e. Figure 11 shows the scaled flow rate versus the pressure gradient β for $a = 0.8$, and three different values of L_e. As we can observe from this figure, the role of L_e is a little more important than in the cavity configuration. Even though the changes in flow rate are not very large, the parameter L_e plays an interesting role. For instance, for $\beta = 10^{2.5}$ (Figure 11(b)), the pipe with $L_e = 0.65$ delivers an increment in flow rate of 69%, i.e.,

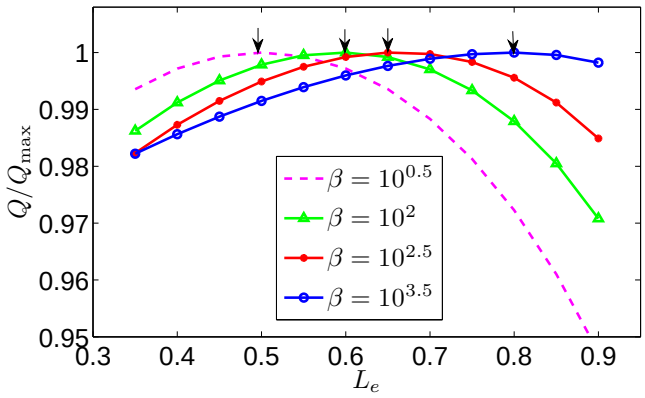

FIGURE 12. Flow rate Q as function of L_e, for sinusoidal pipes with $L = 5$, and different values of β. The flow rates have been scaled by the maximum flow rate $Q_{\max}$ for each value of β.

1% more than the pipe with $L_e = 0.5$. On the other hand, for $\beta = 10^{3.5}$, now the pipe with $L_e = 0.75$, is the best pipe among these three, with an improvement of 36.7% in flow rate, compared to the 35.5% of the pipe with $L_e = 0.5$, and the 36% of the one with $L_e = 0.65$.

The previous observation lets us see that the optimal value of L_e depends on the mean pressure gradient β. This dependency can be seen with more clarity in Figure 12. In this figure we have plotted the flow rates as functions of L_e. For convenience, all values have been scaled by the maximum flow rate, for each value of β. The maximum of each curve appears indicated by an arrow, and from this figure, it is clear that the optimal L_e shifts to the right when β increases, for instance, for $\beta = 10^2$, the largest flow rate is attained around $L_e = 0.6$, and for $\beta = 10^{3.5}$, around $L_e = 0.8$. In the case of small pressure gradients, the optimal value of L_e approaches 0.5. It is also worth mentioning that in all cases, including the cavity configuration, setting L_e below 0.5 is always detrimental, and therefore this should be avoided.

5 CONCLUSIONS

In this paper we presented a numerical approach that allows us to study the effects of wall shape in the flow. With this methodology, we could tackle the problem of optimizing the wall-shape of a periodic section of a pipe, for improving the flow rate for a prescribed pressure gradient. From the two parameters characterizing the geometry, the amplitude a, shows to be the one that can contribute the most for increasing the flow rate. The potential improvement is specially promising when the period is larger than the radius of the pipe. In our study case, we observed an increase in flow rate of up to 120%, for small Reynolds numbers, and of 35%, for large Reynolds numbers. When the period is smaller than the radius, the improvement was about 8%.

The ratio between the expansion and contraction regions, turns out to be irrelevant for the cavity configuration, and in this case, is better to concentrate on finding a convenient value for the amplitude. In practice, one would need to balance the benefit in terms of increase in flow rate, with the extra costs of increasing the amplitude a. In the slowly varying case, the parameter L_e shows a very interesting behavior, which we studied. For large values of the pressure gradient, it is possible to obtain some extra improvement by changing this parameter from 0.5.

In the overall, the possibility of improving the flow rate in corrugated pipes by modifying the wall-shape shows to be very promising for laminar flow cases. The possible advantages for a turbulent flow is currently under study. In the laminar flow case, one guideline we obtain from the present paper is that, it is recommendable to attempt to increase the period of the pipe, in order to benefit the most from wall-shape design. Of course in a practical situation, the benefits of having a larger flow rate, should be balanced with other possible effects and technical restrictions, such as mechanical strength, among others.

ACKNOWLEDGMENT

This work is part of a project in collaboration with Imtech and it is funded by Ballast Nedam IPM.

REFERENCES

[1] Witz, J. A., Ridolfi, M. V., and Hall, G. A., 2004. "Offshore LNG transfer - a new flexible cryogenic hose for dynamic service". Offshore Technology Conference.

[2] Nikuradse, J., 1933. Stormungsgesetz in rauhren rohren, vDI Forschungshefte 361 (English translation: Laws of flow in rough pipes.). NACA Technical Memorandum 1292, National Advisory Commission for Aeronautics, Washington, DC, USA.

[3] Moody, L. F., 1944. "Friction factors for pipe flow". *Trans. ASME*, ***66***(8), November, pp. 97–107.

[4] Lessen, M., and Huang, P., 1976. "Poiseuille flow in a pipe with axially symmetric wavy walls". *The Physics of Fluids*, ***19***(7), July, pp. 945–950.

[5] Inaba, T., Ohnishi, H., Miyake, Y., and Murata, S., 1979. "Laminar flow in a corrugated pipe". *Bulletin of the JSME*, ***22***(171), September, pp. 1198–1204.

[6] Blackburn, H. M., Ooi, A., and Chong, M. S., 2007. "The effect of corrugation height on flow in a wavy-walled pipe". In 16th Australasian Fluid Mechanics Conference, A. Editor and B. Editor, eds., pp. 559–564.

[7] Technip. URL `http://www.technip.com/pdf/OffshoreLNG.pdf`.

[8] Stone, J. B., Ehrhardt, M. E., and Johnston, A. B., e., 2000. Offshore LNG loading problem solved. Tech. rep., GasTech2000.

[9] Cengel, Y. A., and Cimbala, J. M., 2006. *Fluid Mechanics: Fundamentals and Applications*. McGraw Hill.
[10] Herwig, H., Gloss, D., and Wenterodt, T., 2010. "Flow in channels with rough walls-old and new concepts". *Journal of Heat Transfer Engineering,* ***31***(8), pp. 658–665.
[11] Herwig, H., and Wenterodt, T., 2008. "A new approach to understanding and modelling the influence of wall roughness on friction factors for pipe and channel flows". *J. of Fluid Mech.,* ***613***, pp. 35–53.
[12] Povkh, I. L., and Finoshin, N. V., 1989. "Calculating the total resistance for a tube with variable cross section". *Teoreticheskaya i Prikladnaya Mekhanika,* ***21***, pp. 120–124.
[13] Van der Linden, B. J., Ory, E., Dam, J., Tijsseling, A. S., and Pisarenco, M., 2009. "Efficient computation of three-dimensional flow in helically corrugated hoses including swirl". In Proceedings of 2009 ASME Pressure Vessels and Piping Conference. PVP2009-77997.
[14] Pisarenco, M., van der Linden, B. J., Tijsseling, A., Ory, E., and Dam, J., 2009. "Friction factor estimation for turbulent flows in corrugated pipes with rough walls". In Proceedings of the ASME 28th International Conference on Ocean, Offshore and Arctic Engineering, ASME. OMAE2009-79854.
[15] Patankar, S. V., Liu, C. H., and Sparrow, E. M., 1977. "Fully developed flow and heat transfer in ducts having streamwise-periodic variations of cross-sectional area". *ASME J. Heat Transfer,* ***99***, pp. 180–186.
[16] Stel, H., Morales, R. E. M., and Franco, A. T., e., 2010. "Numerical and experimental analysis of turbulent flow in corrugated pipes". *Journal of Fluids Engineering,* ***132***(071203), July.
[17] Reddy, J. N., and Gartling, D. K., 2001. *The Finite Element Method in Heat Transfer and Fluid Dynamics*. CRC Press.
[18] COMSOL, 2006. *User's Guide. COMSOL AB.*
[19] Deiber, J. A., and Schowalter, W. R., 1979. "Flow trough tubes with sinusoidal axial variations in diameter". *AIChE Journal,* ***25***(4), pp. 638–645.
[20] Gadala Maria, F., 1973. The Study of a Model for the Flow of Viscoelastic Fluids through Porous Media. Tech. rep., Department of Chemical Engineering, Princeton University, N. J., USA.
[21] Cotrell, D. L., McFadden, G. B., and Alder, B. J., 2008. "Instability in pipe flow". *PNAS,* ***105***(2), pp. 428–430.

PREVIOUS PUBLICATIONS IN THIS SERIES:

Number	Author(s)	Title	Month
11-13	M.E. Rudnaya H.G. ter Morsche J.M.L. Maubach R.M.M. Mattheij	A derivative-based fast autofocus method	Febr. '11
11-14	E.J.W. ter Maten O. Wittich A. Di Bucchianico T.S. Doorn T.G.J. Beelen	Importance sampling for determining SRAM yield and optimization with statistical constraint	Febr. '11
11-15	R.V. Polyuga A. van der Schaft	Model reduction of port-Hamiltonian systems based on reduction of Dirac structures	Febr. '11
11-16	S. Gugercin R.V. Polyuga C. Beattie A. van der Schaft	Structure-preserving tangential-interpolation based model reduction of port-Hamiltonian systems	Febr. '11
11-17	P.I. Rosen Esquivel J.H.M. ten Thije Boonkkamp J.A.M. Dam R.M.M. Mattheij	Numerical wall-shape optimization for laminar flow in corrugated pipes	Febr. '11

Ontwerp: de Tantes,
Tobias Baanders, CWI